Ocean Engineering 188 (2019) 106226

Contents lists available at ScienceDirect

Ocean Engineering

journal homepage: www.elsevier.com/locate/oceaneng

Structural health monitoring of towers and blades for floating offshore wind turbines using operational modal analysis and modal properties with numerical-sensor signals

Hyoung-Chul Kim [a,*], Moo-Hyun Kim [a], Do-Eun Choe [b]

[a] Ocean Engineering Department, Texas A&M University, College Station, TX, 77843, USA
[b] Civil and Environmental Engineering Department, Prairie View A&M University, Prairie View, TX, 77446, USA

ARTICLE INFO

Keywords:
Operational modal analysis
Floating offshore wind turbine
Health monitoring
Damage detection
Curvature mode shape
Numerical sensor
Turbine-floater-mooring coupled dynamics simulation

ABSTRACT

In the present study, a structural health monitoring (SHM) method for floating offshore wind turbines (FOWTs) is suggested and tested using operational modal analysis (OMA) with numerical-sensor signals. The numerical accelerometer signals along the tower and blade of FOWT in dynamic wind field are used for the OMA. The numerical-sensor signals are simulated using a time-domain turbine-floater-mooring fully-coupled dynamic simulation computer program. To perform the SHM of a FOWT through OMA, natural frequencies, displacement mode shapes (DMS), and curvature mode shapes (CMS) of the tower and blades are obtained and analyzed. The modal properties are systematically compared between the intact and damaged conditions. Their differences are used for damage detection. The results show that CMS is found to be the most effective modal property to detect damage locations and intensities. The performance of the damage detection based on the OMA-CMS analysis is verified by independent FEM (finite element method) results. This study is unique in that the SHM using OMA and CMS for FOWTs is implemented including the floater-tower-blade coupling effects. The technology can contribute to the design of remote SHM system for future FOWTs. A further validated model with field data may build up a huge database for various damage scenarios so that it can be applied to digital-twin-based smart health monitoring technology.

1. Introduction

Despite various advantages of the floating offshore wind turbine (FOWT), it is still slow for it to be commercialized. Currently, FOWTs installed in the real field are only a few, and most of them are just for the test. One of the disadvantages of FOWTs is related to operation and maintenance cost (OPEX). The predictions of the dynamics associated with moored system are more challenging than those associated with fixed one, which yields the large uncertainties and higher costs in the floating-type turbine system compared to the fixed-type turbine system. (Levitt et al., 2011; Moné et al., 2015). One way to reduce the uncertainty and OPEX is the remote structural health monitoring (SHM). By continuously monitoring the sensor signals of the tower or blade, the on-site maintenance schedule can be more flexible, and the inspection intervals can be increased (Hameed et al., 2009). Besides, catastrophic failures and secondary damages can be prevented by early detecting initial damage. If the tower or blades are fully broken, the repair cost is dramatically increased because the entire or partial FOWT units need to be transported to on-land (Griffith et al., 2012).

Nowadays, operational modal analysis (OMA) is a well-accepted method to estimate the modal identification of a structure under actual operating conditions by examining the sensor signals of responses. Therefore, any artificial excitation, such as hammer test, is not needed. By using OMA, the change of the modal natural frequencies, traditional mode shape, and curvature mode shape (CMS) can be estimated. By observing the magnitude of difference in modal characteristics between intact and damaged conditions, structural damages can be detected.

The OMA has been used for bridges (Conte et al., 2008; Magalhães, 2012; Brownjohn et al., 2007, 2010) and on-land wind turbines. White (2010) and Manzato et al. (2014) measured the modal properties of the Micon 65/13M on-land wind turbine with a CX-100 rotor blade using OMA, and they showed that the OMA results agreed with the hammer test results. Tcherniak et al. (2013) and Chauhan et al. (2011) also

* Corresponding author.
E-mail address: doriduul@tamu.edu (H.-C. Kim).

https://doi.org/10.1016/j.oceaneng.2019.106226
Received 7 March 2019; Received in revised form 15 July 2019; Accepted 16 July 2019
Available online 1 August 2019
0029-8018/Published by Elsevier Ltd.

showed the feasibility of the OMA by applying it to the Vestas 225 kW V27 on-land wind turbine and the 3 MW ALSTOM wind turbine, respectively.

This method has also been used for offshore structures. In various offshore fixed wind farms, the modal properties of wind turbines are measured using the OMA (Van der Valk and Ogno, 2014; Devriendt et al., 2012, 2013; De Sitter et al., 2013). Liu et al. (2015), Kim et al. (2015), and Mieloszyk et al. (2015) applied OMA to the jacket type offshore platform, the segmented ship, and the tripod submerged structure, respectively. Additionally, Ruzzo et al. (2016) have measured the modal properties of 6DOF motions of a spar floater using the OMA.

The advancement of OMA for on-land wind turbines has been made by several researchers. Siebel et al. (2012) performed a model test for a small-scaled on-land wind turbine. They measured the acceleration on the tower in the operational condition and estimated the modal properties of the tower using OMA. They showed that the combination of the OMA and the damage detection method based on CMSs was feasible in the real small-scale wind turbine excited by ambient vibration.

Di Lorenzo et al. (2016) used the vibration-based SHM for detecting blade damage. An experiment for obtaining modal properties was performed, and the modal properties of multi-layered blades were estimated using the OMA. The OMA results were compared to the finite element method (FEM) results for validation. Then, the validated FEM model was used for detecting the local damage of blades by observing the CMS including blade rotation effect.

Devriendt et al. (2014) and Weijtjens et al. (2017) proved that the vibration-based health monitoring is effective to detect blade icing or blade damage. They analyzed the collected data of 15-year vibration measurements on five monopile offshore wind turbines with many accelerometers on them. They showed how wind condition affected the vibration phenomenon of the turbine and investigated the interaction effect between wind loads and the blade-tower dynamics. Besides, they obtained the first and second fore-aft and side-to-side mode shapes of the tower, resonance frequencies, and damping value using automated OMA.

Regarding the mode shapes, Pandey et al. (1991) showed that the CMS might be better than the displacement mode shape (DMS) in determining the damage location in a beam. Wang et al. (2014) used the FEM for modal analysis and dynamic-response analysis. The calculated aerodynamic force is applied to the FE model. Through the modal frequency response under aerodynamic wind load, the natural frequencies and mode shapes are estimated and compared to those in damaged condition. They also used the difference in CMS for damage detection as well as the DMS. This study showed that the difference in CMS could more precisely catch the damage location.

So far, SHM studies for FOWTs with physical sensors are hard to find. However, numerical simulations and numerical sensors can be used for the design of SHM system for FOWTs. In the numerical simulation, various damaged conditions can easily be considered, and extensive comparison studies between 'pre-damage' and 'post-damage' states can be performed ahead of the actual measurement in the real-field. The general processes and algorithms of SHM for FOWTs can be economically developed using numerical simulations and numerical sensors. Of course, there are several limitations when using numerical sensors such as measurement noise and variation caused by the environmental and operational factors such as wind speed, temperature, rotational speed, and blade pitch (Hu et al., 2015). However, through the noise-filtering technique, their differences can be reduced (Sainz et al., 2009). Also, the key environmental and operational factors and their effects on modal properties can be included in the numerical modeling.

In this paper, the SHM method using numerical simulations, numerical sensors, OMA, and the difference in CMS is applied to a FOWT. The numerical sensor signals are obtained from turbine-floater-mooring fully-coupled dynamics simulation program in the time domain (Bae and Kim, 2013, 2014a; Bae et al., 2017). The author-developed coupled dynamic-simulation tool has extensively been verified through comparisons with several experiments (Kim et al., 2017; Kim and Kim, 2015). As far as the authors know, the use of OMA and CMS for the SHM of FOWT's including all of their coupling effects cannot be found in the open literature. The modal properties, such as natural frequencies, DMSs, and CMSs, are estimated using the OMA of numerical-sensor signals. The modal properties are systematically compared between the intact and damaged conditions, and their differences are used for local-damage detection. Especially, the CMS and natural frequency are used as the primary indicator for finding the damage location and intensity. The OMA results are double-checked using the independent calculation based on commercial FEM code.

2. Methods

The present SHM method for the FOWT is divided into four-parts like below. First, OMA with time-domain numerical simulations for FOWT is verified. The verification is performed by comparing the modal properties of the intact tower and blade obtained from OMA with those obtained from FEM model. Second, the effects of non-linear mooring stiffness, wave, and coupling between tower and blades on the modal properties in time-domain simulations and FEM analysis are investigated. Third, the SHM of the tower is carried out. The mode shapes and natural frequencies are compared between the intact (or 'pre-damage') and damaged (or 'post-damage') conditions in the frequency-domain FEM analysis. Then, the time-domain simulation/analysis is carried out. By applying frequency-domain decomposition (FDD), which is one method of OMA, to the acceleration results obtained from the time-domain numerical sensors, the natural frequencies and CMSs are estimated, and the dynamics of blades and tower are analyzed in the intact and damaged conditions. Through the differences in the modal properties between the intact and damaged conditions, the damaged location can be detected, and the intensity of damage can be estimated. Additionally, the FEM results can also be used for the verification of the changes of modal properties obtained from the OMA. Lastly, the SHM of the blade is carried out in the parking condition, which can be so during the periodic maintenance period, using the developed OMA. The numerical simulations and the corresponding OMA with blades rotating and controlled is to be detailed in the authors' sequel paper. The exemplary analysis chart for the present SHM is given in Fig. 1. The concepts about OMA and difference in CMS are introduced in the next two sections.

2.1. Operation modal analysis (OMA) - frequency domain decomposition (FDD) method

The FDD, which was first suggested by Brincker et al. (2001), is an output-only modal analysis technique in the frequency domain. Through this method, modal properties can be estimated from the output Power Spectral Densities (PSD) gained in the white noise loading condition. The PSD matrix of the output response for each frequency can be decomposed by applying the singular value decomposition to the PSD matrix. As a result, modal properties, such as the natural frequencies and mode shapes, are obtained:

$$G_{xx}(\omega_i) = U_i S_i U_i^H \tag{1}$$

where $G_{xx}(\omega_i)$ is an output PSD matrix, S_i is a diagonal matrix which includes singular values and U_i is the unitary matrix that includes singular vectors. Singular values can be acquired from the output response, and the singular values of the PSD matrix are plotted in the frequency domain. The dominant peaks displayed in the plotted graph mean the natural frequencies, and mode shapes can be estimated by finding the corresponding singular vectors of the singular values. The detailed information of FDD techniques is given by (Brincker et al. (2001)).

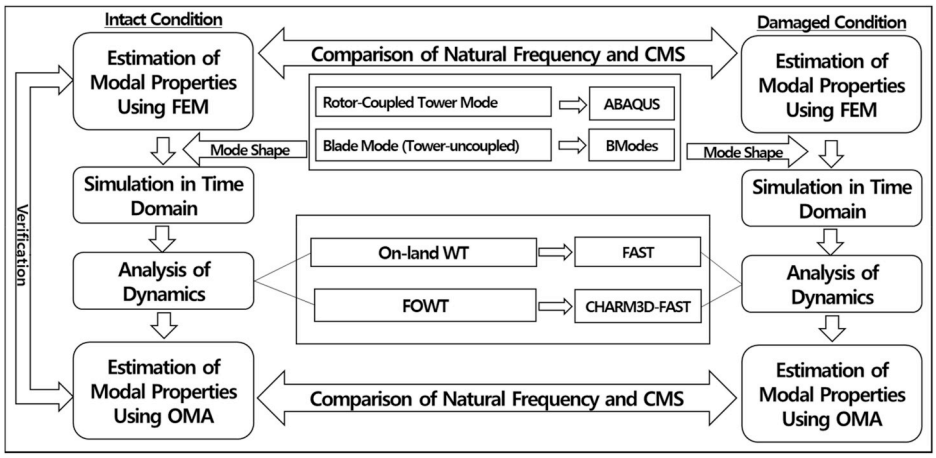

Fig. 1. Process of modeling, verification, and damage detection of wind turbine.

2.2. Difference in CMS (curvature mode shape) as the indicator of damage detection

For the simulation of SHM, numerical accelerometers along the blade/tower length are installed. The acceleration is measured in the time domain on each location. Using the OMA method, the modal characteristics of blade/tower, such as natural frequencies and mode shapes, are estimated. When a structure is damaged, the stiffness on the damaged region decreases, which causes the change of the modal characteristics of the structure. The damage can be detected by comparing the difference in the modal characteristics between intact and damaged conditions. The displacement mode shape (DMS) is usually used for damage detection (Schulz et al., 2003). Pandey showed that the CMS might sometimes be better than DMS (Pandey et al., 1991; Wang et al., 2014). Curvature can be defined as follows:

$$\kappa = \phi'' = \frac{M}{EI} \tag{2}$$

where ϕ is DMS, M is the bending moment, E is Young's modulus, and I is the second moment of the cross-sectional area.

3. Numerical model

3.1. Configurations of 5 MW DeepCWind FOWT and on-land wind turbine

Fig. 2 shows the 5 MW DeepCWind FOWT and on-land wind turbine,

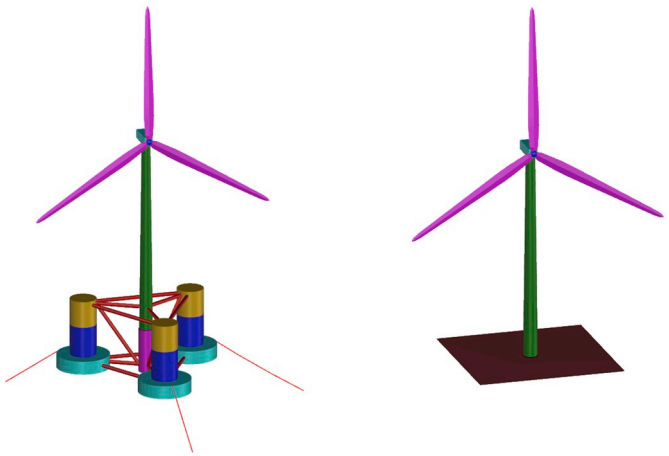

Fig. 2. DeepCwind semisubmersible FOWT (a) and on-land wind turbine (b).

respectively. The property of the floating platform excluding the wind turbine part is given in Table 1. The wind turbine is based on the NREL 5 MW baseline turbine, and the detailed material properties of blade and tower are presented in the NREL technical report by Jonkman et al. (2009). For the on-land wind turbine, the same wind-turbine is used for the comparison to the FOWT case, and it is assumed that the tower is fixed at the bottom. The wind-turbine-related mass properties used in the FEM analysis and the time-domain analysis are tabulated in Table 2 and Table 3. The platform added mass is also given in Table 1. The added mass of FOWT is obtained from the frequency-domain potential-theory-based 3D diffraction/radiation program. About the mooring-line modeling, three catenary mooring lines are installed for the FOWT, and the high-order finite-rod-element method was used for the mooring dynamics in the time-domain analysis. The mooring stiffness and hydrostatic stiffness are obtained from the static offset test, and they are summarized in Table 4.

3.2. FEM analysis

The mode shapes of the blade and tower are pre-calculated using FEM modal analysis. For the modal analysis in the frequency domain, both blade-tower-semi-coupled BModes-FEM (sub-program in FAST) and blade-tower-fully-coupled ABAQUS-FEM programs are used for double-checking. In the case of blade, differences between the two results are negligible. In the case of tower, the fully-coupled effect is not ignorable. This difference can affect the ensuing OMA results. Therefore, ABAQUS-FEM is used for the tower, and BModes-FEM is used for the blade in the subsequent OMA. In the ABAQUS modeling, the actual three blades are modeled as beam elements, and only the hub and nacelle are assumed as point mass and inertia as shown in Fig. 3. The point mass properties of tower top, nacelle, and hub are summarized in Table 2. In case of FOWT, the added mass and added inertia of platform, hydrostatic restoring force/inertia, actual mass and inertia of platform, and the

Table 1
Platform mass and added mass properties in ABAQUS.

Title	Unit	Value
Platform Mass	kg	1.344E+07
Ixx from MWL	kg-m^2	6.827E+09
Iyy from MWL	kg-m^2	6.827E+09
Izz form MWL	kg-m^2	1.226E+10
Platform Added Mass Max	kg	6.248E+06
Platform Added Mass May	kg	6.248E+06
Platform Added Mass Maz	kg	1.432E+07
Platform Added Ixx	kg-m^2	7.192E+09
Platform Added Iyy	kg-m^2	7.192E+09
Platform Added Izz	kg-m^2	4.823E+09

Table 2
Tower top point mass properties in BModes FEM program.

Title	Unit	Value
Tower Top Height from MWL	m	87.600
Z of Tower Top CM from MWL	m	89.567
X of Tower Top CM from Tower Center Line	m	−0.414
Y of Tower Top CM from Tower Center Line	m	0.000
Ixx from Tower Top CM	kg-m^2	3.865E+07
Iyy from Tower Top CM	kg-m^2	2.350E+07
Izz from Tower Top CM	kg-m^2	2.535E+07
Ixy from Tower Top CM	kg-m^2	−1.300E+06

Table 3
Nacelle and hub point mass properties in ABAQUS.

Title	Unit	Value
Nacelle mass	kg	240000
Izz from Nacelle CM	kg-m^2	2.608E+06
Hub Mass	kg	56780
Ixx from Hub CM	kg-m^2	1.159 E+05

Table 4
Mooring stiffness and hydrostatic stiffness used in ABAQUS.

Title	Unit	Value
Surge Mooring Stiffness	N/m	7.099E+04
Sway Mooring Stiffness	N/m	7.012E+04
Heave Mooring Stiffness	N/m	1.942E+04
Roll Mooring Stiffness	N-m/rad	8.670E+07
Pitch Mooring Stiffness	N-m/rad	8.670E+07
Yaw Mooring Stiffness	N-m/rad	1.163E+08
Heave Hydrostatic Stiffness	N/m	3.730E+06
Roll Hydrostatic Stiffness	N-m/rad	1.070E+09
Pitch Hydrostatic Stiffness	N-m/rad	1.070E+09

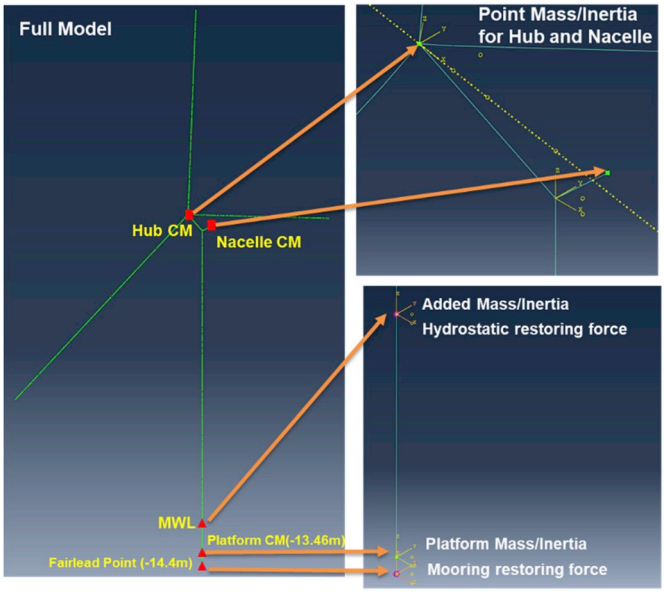

Fig. 3. Combined tower and blade modeling using ABAQUS with actual three blades in FOWT.

mooring stiffness are entered with respect to the platform center of mass CM in ABAQUS as shown in Fig. 3. The values are summarized in Tables 1 and 4. The blade-tower-fully-coupled ABAQUS-FEM results were double checked against ADAMS-FEM-program results by Di Lorenzo et al. (2013) and the two independently calculated results for the same wind tower and blades agree very well.

3.3. Time-domain coupled model

In the FOWT dynamic analysis, hydro-dynamic loading and mooring tensions are obtained from CHARM3D. They are fed to FAST at each time step. Then FAST fills out the forcing function of the platform DOFs using those forces, and solves displacements, velocities, and accelerations of all the degrees of freedom including elastic responses of towers and blades. The obtained platform displacement and velocity data are then fed into CHARM3D side to update the relevant external forces. The exemplary combined left-hand-side matrix for the coupled dynamic analysis has total 24 DOFs including six DOFs for platform rigid body motion, four DOFs for tower flexibility, three DOFs for flexibility of each blade, and five DOFs for nacelle yaw, rotor furl, generator azimuth, tail furl, and drive train flexibility. More details of the numerical modeling of the platform and mooring are referred in (Kim and Kim (2015); Bae and Kim (2014b)).

For the implementation of the dynamics caused by the elasticity of tower and blade in time domain simulation, the ElastoDyn, subroutine module of FAST, is used. In ElastoDyn, the modal-based dynamic formulations are used for employing the blade and tower elasticity, and the nonlinear equations of motions are derived and implemented using Kane's dynamics. The pre-calculated mode shapes include the first and second fore-aft tower modes, first and second side-to-side tower modes, the first and second flap blade modes, and first edge blade mode. They are specified as polynomial coefficients and entered to the FAST time-domain simulation. The mode-shape polynomial equations are used as shape functions in a nonlinear beam model using the Rayleigh-Ritz method.

3.4. Time-domain simulation

The time-domain numerical simulation is carried out using FAST v7 for the on-land wind turbine and using CHARM3D-FAST for the FOWT. The simulations are carried out in the parking (blade-fixed) condition without blade rotation and control, for simplicity. In total, 25 and 19 numerical sensors are installed along the tower length and blade length respectively, and their locations are tabulated in Table 5. Many numbers of numerical sensors enough to detect any damaged locations are used for examining the feasibility of this method. The optimization of the number of sensors can be discussed in a follow-up study. In the case of physical sensors, there may exist unwanted noises in the sensor signals, but in the present study, by using numerical sensors, this is not considered. The full-field wind is generated using the Turbsim program (Jonkman, 2009), which is a stochastic, full-field, turbulent-wind simulator using various wind spectra and turbulence models. For the implementation of turbulence, the Kaimal turbulence model is used. The average wind speed, turbulence intensity, and the vertical power law exponent of wind data used in the simulation are 6.15 m/sec, 8%, and 0.1, respectively. If the turbulence is included in the wind speed data, the wind spectrum becomes very similar to the white noise spectrum in the high-frequency range. In the simulation, the wind speed varies in all directions (x, y, and z directions) because of the turbulence effect. This also means that the wind causes the excitations on the blade and tower in all directions.

The accelerations of fore-aft and side-to-side directions are obtained from the numerical sensors. Based on the acceleration results, the graphs of the first singular value of the PSD matrix are plotted in Fig. 4. The yellow and green portions of the figures represent the 1st tower mode and the 2nd tower mode, respectively. Other excitations are generated by 6DOF platform motions and the blade modes. In the FOWT, the same wind data is used as that used in the on-land case. The sea condition is assumed to be still water, i.e. the platform dynamics result from dynamic wind loadings. Wind forces including wind turbulence are more desirable for OMA since they have broadband spectra (Tcherniak et al., 2011; Osgood et al., 2011). In Section 4.2.2, it is shown that the additional wave effect on the OMA and modal properties of the tower is minimal, i.

Table 5
Locations of numerical sensors at the blade and tower.

	Location of sensors (m)
Tower (From tower base)	0.4, 1.3, 2.2, 3.9, 8.3, 12.7, 17.1, 21.4, 25.8, 30.2, 34.6, 38.9, 43.3, 47.7, 52.1, 56.4, 60.8, 65.2, 69.6, 73.9, 78.3, 82.7, 85.3, 86.2, 87.1
Blade (From blade root)	0.0, 1.4, 4.1, 6.8, 10.3, 14.4, 18.5, 22.6, 26.7, 30.8, 34.9, 39.0, 43.1, 47.2, 51.3, 54.7, 57.4, 60.1, 61.5

e. the same OMA results can be obtained with waves.

4. SHM process

4.1. Verification of developed numerical models for FOWT

Dynamic behavior caused by the elasticity of tower and blade is very complicated. The reason is that three rotor blades are connected to the hub allowing rotation with respect to the drive-train axis in the nacelle, which is connected to the tower, and they are dynamically coupled. Because of this complication, various structural modes are generated in the modal analysis. By using the OMA or FEM programs, various tower and blade modes can be found in the given condition, and their mode shapes are displayed in Fig. 5 and Fig. 6. In the on-land case, the presently calculated natural frequencies of modes mentioned above are compared between FEM and OMA. The OMA results are obtained through the numerical-sensor signals from time-domain simulations. Their average difference of all the modes is 2%. Besides, the present ABAQUS-based-FEM results were double-checked against Di Lorenzo et al. (2013) ADAMS-based-FEM results for the same wind turbine. The comparison is tabulated in Table 6, and the frequencies of tower and blade agree well with each other.

For the FOWT case, the same wind turbine is mounted on the floating base instead of land. As far as the authors know, there is no SHM study for FOWTs in the open literature by utilizing coupled-system numerical simulations, FEM, and OMA. Before going into the details of FOWT results, the natural frequencies of the tower and blade modes of FOWT are compared with those of on-land wind turbine. This shows the effects of foundation on the modal properties of the wind turbine. First, the modal properties of tower are compared using FEM (ABAQUS). As shown in Fig. 7, there is little difference in the second mode between them, but larger discrepancies can be observed in the natural frequencies of first tower modes, i.e., that of FOWT is increased by 13.0–15.5% compared to the on-land case. This difference is mainly caused by the boundary condition of the tower base (Bir and Jonkman, 2007). In the case of blade modes, there is little difference in the natural frequencies of the first flap and first edge modes between on-land wind turbine and FOWT, but the natural frequencies of FOWT's second flap mode are 2–3% greater than those of on-land wind turbine, as shown in Fig. 8 and Table 7. These results show that using a floating base more influences the tower mode than blade mode.

Next, the applicability of OMA for FOWT is tested. In this regard, the natural frequencies are obtained using the ABAQUS software, and the results are compared against those from the OMA with the CHARM3D-FAST time-domain simulation results. As shown in Table 8 and Fig. 9 ~ Fig. 10, the FEM results agree well with the OMA results. The maximum difference is 3.1% in the second blade pitch mode. It means that the OMA analysis can reliably catch the modes of blade and tower even for the FOWT.

4.2. Effects of nonlinear mooring stiffness, wave, and coupling between tower and blade on wind turbine modes

4.2.1. Mooring stiffness effect

The actual mooring stiffness for the FOWT can be obtained from the numerical static-offset test. In the surge and sway, the corresponding mooring stiffness increases with displacements showing nonlinear hardening behavior (Kim and Kim, 2015). This nonlinearity can change the surge and sway stiffness when they are large. In CHARM3D-FAST numerical simulation, the actual mooring is modeled as it is. However, in ABAQUS-FEM modeling, the actual mooring is modeled by equivalent linear spring, so the equivalent spring may not be accurate when surge-sway are large, which may affect the accuracy of modal-property comparison between the two. For the present case study, however, the effects turn out to be negligible. The natural frequencies of the tower modes are estimated with various mooring stiffness within 100% of variation using ABAQUS, and the resulting change in natural frequencies is less than 0.1% in the first ten modes based on the FEM analysis results. This means that the nonlinear behavior of FOWT's mooring stiffness in the expected range of surge/sway does not significantly affect the modal properties of tower and blade.

4.2.2. Wave effect on tower mode

Let us also consider the effects of sea waves in the assessment of natural frequencies and mode shapes of FOWT tower and blade through OMA. In the present case study, only dynamic wind loadings were given,

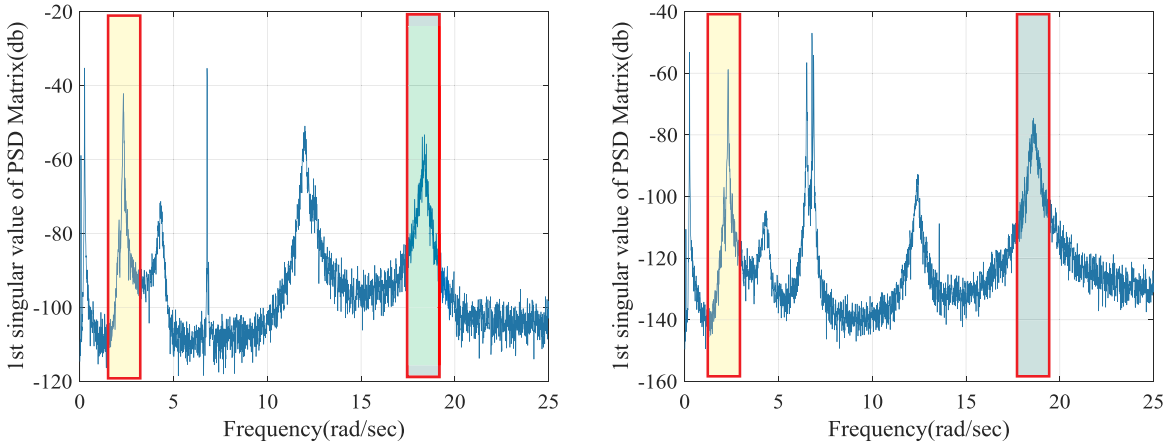

Fig. 4. 1st singular value of PSD Matrix of fore-aft tower mode (A) and side-to-side tower mode (B) in FOWT.

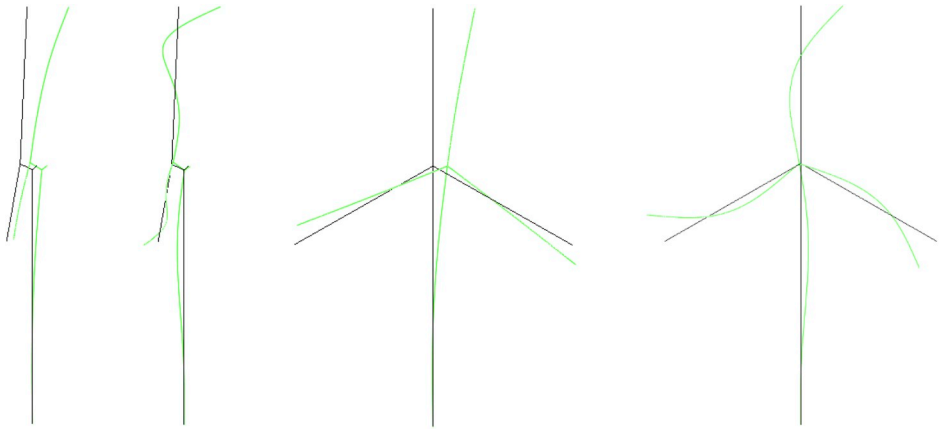

Fig. 5. Tower FA 1st and 2nd modes and Tower SS 1st and 2nd modes (green line is deformed shape, and black is undeformed shape). (For interpretation of the references to colour in this figure legend, the reader is referred to the Web version of this article.)

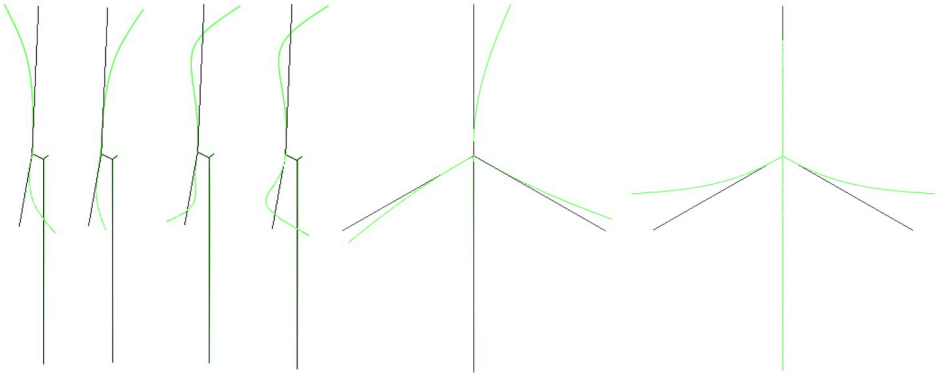

Fig. 6. Blade flap 1st pitch and sym, 2nd pitch and sym, and Blade edge 1st pitch and Yaw mode shapes (green line is deformed shape, and black is undeformed shape). (For interpretation of the references to colour in this figure legend, the reader is referred to the Web version of this article.)

Table 6
Comparison of natural frequencies of tower and blade for the on-land WT between ADAMS (FEM) and ABAQUS (FEM).

Mode (rad/sec)	ADAMS (FEM)	ABAQUS (FEM)	Diff (%)
Tower 1st fore-aft	1.985	2.264	−0.96
Tower 1st side to side	2.004	2.261	0.20
Blade 1st flap pitch	4.203	4.163	0.95
Blade 1st flap sym	4.441	4.336	2.36
Blade 1st edge pitch	6.635	6.78	−1.34
Blade 1st edge yaw	6.654	6.865	−2.13
Blade 2nd flap pitch	11.662	11.601	0.65
Blade 2nd flap sym	12.315	12.221	0.77

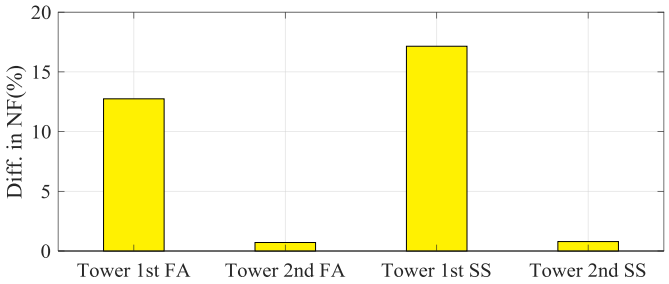

Fig. 7. Differences in natural frequencies of tower modes between on-land and FOWT.

and the corresponding OMA was carried out to obtain the modal properties. In this regard, the OMA of the FOWT with additional irregular waves is also tested. JONSWAP spectrum with significant wave height $H_s = 2$m, peak period $T_p = 7.5$s, and enhancement parameter $= 2$ was used for the generation of uni-directional irregular waves. The two OMA results were compared. In both cases, the same wind excitations were used. The comparison is summarized in Table 9. We see little difference between the two cases, which is somewhat expected because the modal properties of the tower and blade do not change according to the input force. Also, typical linear wave frequencies are far from the typical wind-turbine natural frequencies, and the effect of second-order sum-frequency wave excitation on the dynamics of the wind turbine is significantly low compared to the effect of wind turbulence. Since both cases produce almost identical results, from this point on, irregular waves are not considered, and only dynamic wind excitations are inputted in the ensuing FOWT simulations.

4.2.3. *Coupled effect between tower and blade*

To evaluate the rotor-coupled effects on the tower modes, two comparison studies are carried out, and the results are displayed in Fig. 11. The first is the comparison of natural frequencies of the tower obtained from FEM between when the rotor is simplified to be the top point mass and inertia (FEM-Sim) and when the full rotor blades are included as the beam elements (FEM-Full). A considerable difference in the natural frequencies of second tower modes is shown. The second is the comparison of the natural frequencies of the tower between OMA and FEM when the mode shapes obtained from the simplified FEM are entered to the time-domain analysis. The OMA results (OMA-Sim) show appreciable differences in the second modes compared to FEM analysis

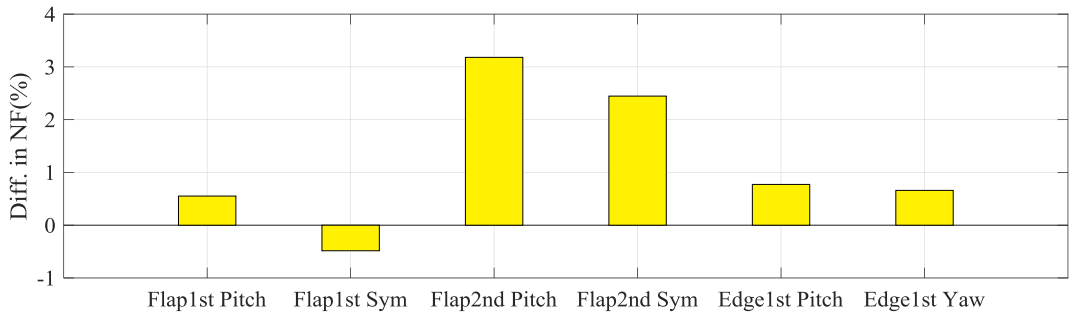

Fig. 8. Differences in natural frequencies of blade modes between on-land and FOWT.

Table 7
Comparison of tower natural frequencies between the on-land wind turbine and FOWT.

Mode (rad/sec)	On-land	FOWT
FA1st	1.971	2.316
SS1st	1.971	2.309
FA2nd	18.247	18.377
SS2nd	18.454	18.600

Table 8
Comparison of natural frequencies of tower and blade modes for FOWT between the FEM and OMA.

Mode (rad/sec)	ABAQUS (FEM)	FAST-CHARM3D (OMA)
Tower 1st fore-aft	2.264	2.316
Tower 1st side to side	2.261	2.309
Blade 1st flap pitch	4.163	4.188
Blade 1st flap sym	4.336	4.318
Blade 1st edge pitch	6.780	6.780
Blade 1st edge yaw	6.865	6.865
Blade 2nd flap pitch	11.601	11.970
Blade 2nd flap sym	12.221	12.520
Tower 2nd fore-aft	17.905	18.377
Tower 2nd side to side	17.794	18.600

results (FEM-Full). However, the mode shapes obtained from full rotor modeled FEM are entered, the OMA results (OMA-Full) agree well with the FEM results (FEM-Full). This means that the rotor-coupled effect is appreciable in the second mode of the tower; thus, the rotor-coupled tower mode shapes must be entered to the time-domain simulation for obtaining the accurate tower modal properties through OMA.

In the case of blade, the tower-coupled effect is not included in the pre-calculated blade mode shapes, which means the blade is assumed to be fixed-free beam. The uncoupled blade mode shapes are plugged into the time-domain simulation, and the natural frequencies of blade are estimated from the OMA. Even though the tower-coupled effect is not included in the pre-calculated blade mode shapes, the actual tower-blade-coupling effect is considered in the time-domain simulation. The natural frequencies of blade obtained from the OMA are compared to the natural frequencies obtained from FEM (FEM-ABAQUS) including tower coupled effect. As shown in Fig. 12 and Fig. 13, the differences in natural frequencies of the 1st and 2nd blade modes obtained by FEM-ABAQUS and OMA are significantly low. Besides, the other FEM results (FEM-ADAMS) presented by Di Lorenzo et al. (2013) agree well with our FEM and OMA results. This infers that the tower-coupled effect on the blade mode shape doesn't affect much the OMA results of the first two blade modes.

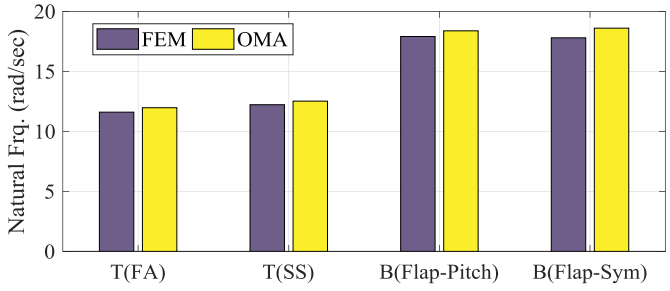

Fig. 10. Comparison of natural frequencies of 2nd modes in FOWT between the FEM and OMA.

Table 9
Comparison of tower natural frequencies of the FOWT between still water and 2m significant height wave.

Mode (rad/sec)	Still Water	With Wave
FA1st	2.316	2.324
SS1st	2.309	2.301
FA2nd	18.377	18.377
SS2nd	18.600	18.570

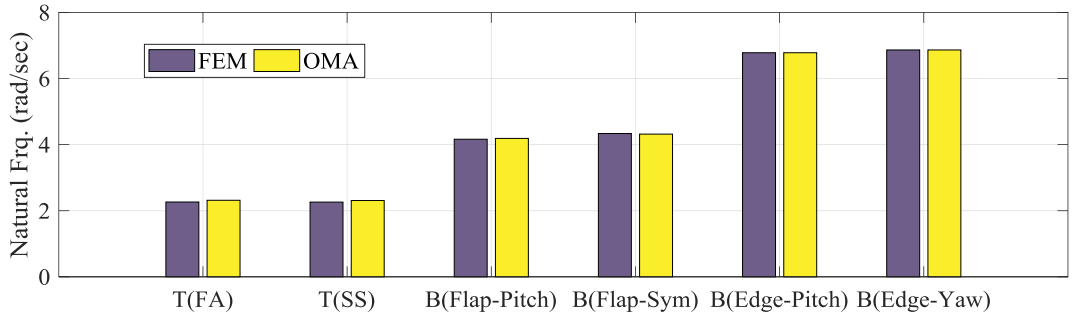

Fig. 9. Comparison of natural frequencies of 1st modes in FOWT between the FEM and OMA.

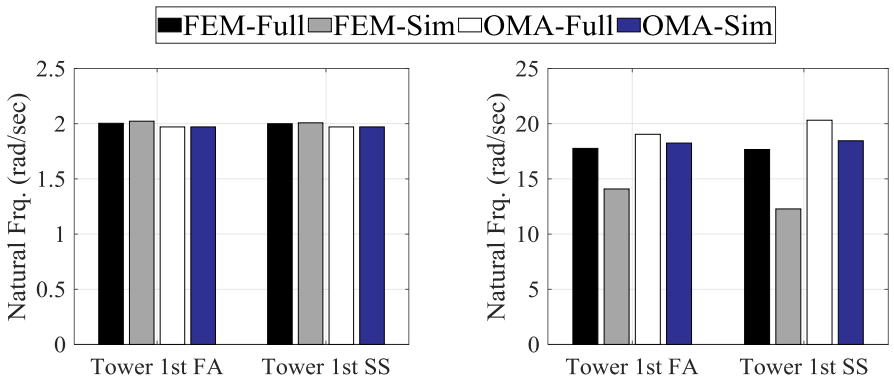

Fig. 11. Natural frequencies of the 1st tower FA and SS (A) and the 2nd tower FA and SS (B) in various analyses.

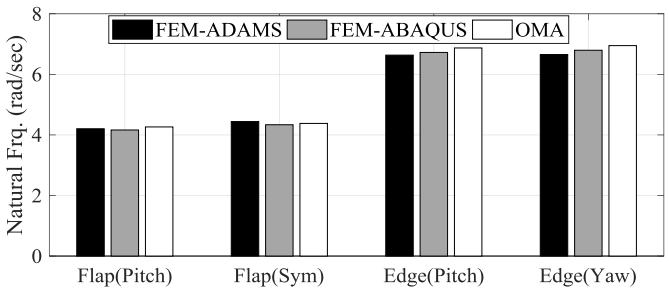

Fig. 12. Natural frequencies of the 1st blade modes in various analyses.

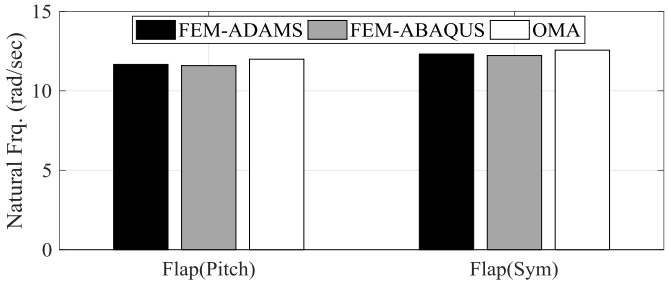

Fig. 13. Natural frequencies of the 2nd blade modes in various analyses.

4.3. Structural health monitoring

4.3.1. Modeling of damaged tower and blade in the simulation by the reduction of stiffness

Various damage types of blade/tower have been reported. Poor-quality control, improper installation, lightning, fire, and strong wind have been blamed for the structural damage of blade and tower. Typical damages in turbine blades are splitting and fracture, cracks, and the de-bonding of the adhesive layer and joint with fatigue damage (Ciang et al., 2008; Sørensen et al., 2004; Shokrieh and Rafiee, 2006). The initial crack development can be modeled by the reduction of local stiffness (Griffith et al., 2012; Shokrieh and Rafiee, 2006; Kim et al., 2014). Therefore, in the present study, the damaged condition is implemented by reducing the stiffness of the damaged part in the FEM modal analysis and the subsequent fully-coupled time-domain simulation. For example, 10% and 30% damaged conditions at some position mean that the stiffness of the specific damaged location is decreased by 10% and 30%, respectively. The reduced stiffness at a specific point is assumed to gradually vary with distance so that it matches with the original value of ambient parts. The damaged positions are started from tower/blade base and normalized by the entire length. For example,

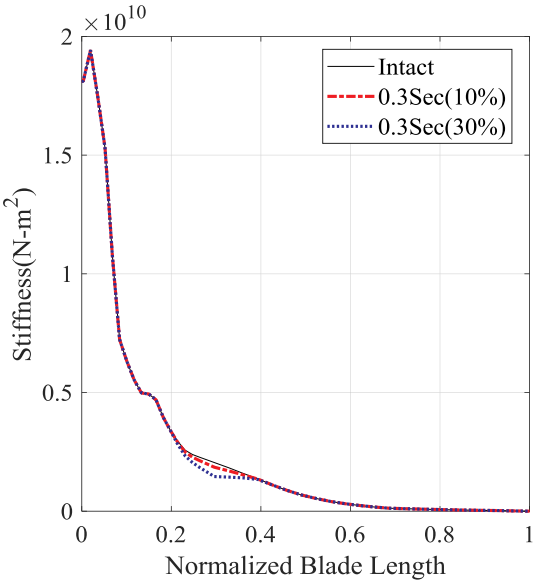

Fig. 14. Decrease in flap bending stiffness of blade when 10% and 30% damages occur at the 0.3 section of the blade.

when damage develops at 0.3 section of the tower, the damage occurs at the location of 30% of total tower length from the tower base. The exemplary stiffness variation along the blade for 10% and 30% damage is shown in Fig. 14.

In the next section, the presumed local damage is modeled by the fully-coupled ABAQUS-FEM to obtain the corresponding elastic modes, which in turn is used in the fully-coupled CHARM3D-FAST dynamic simulation to generate numerical-sensor signals. Then, the numerical-sensor signals are used in the OMA with CMS to check whether the inputted local damage can correctly be recovered. In real health-monitoring system, we only get signals from physical sensors. Then by applying the present OMA-CMS algorithms, the structural problem can be detected from the shift of natural frequencies and the difference in curvature mode shapes. Then, the severity of the damage can be judged from the computer-generated big-database generated for numerous damage scenarios. The correspondence between the actual damage scenarios and the numerically modeled scenarios also needs to be investigated.

4.3.2. Structural health monitoring of FOWT-tower using FEM

Each damage of tower is assumed to happen at 0.1, 0.3, 0.5, 0.7, and 0.9 sections from the tower base, respectively. The stiffness reduction of 10% and 30% is considered for each case. The natural frequencies and the mode shapes are compared between intact and damaged conditions

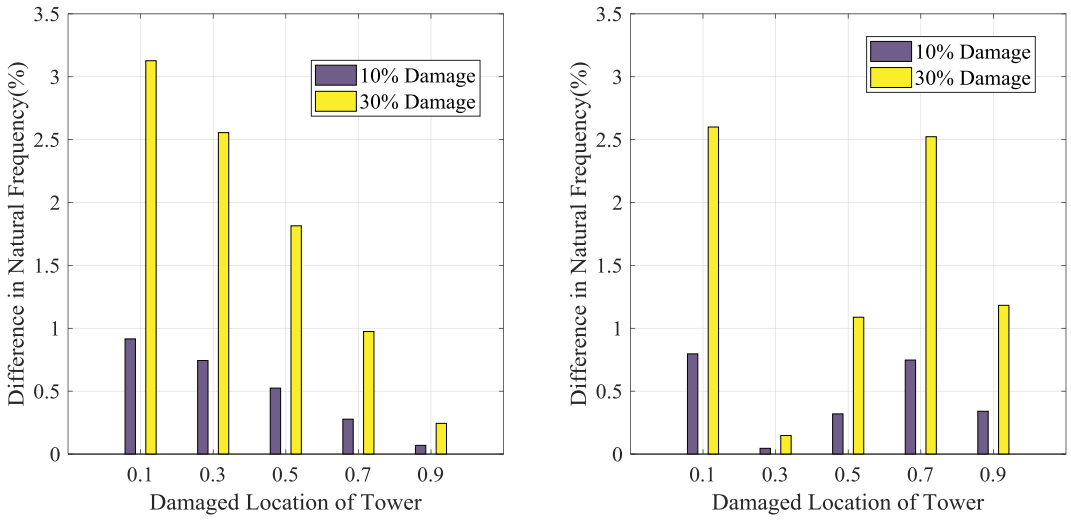

Fig. 15. Difference in natural frequencies of tower fore-aft 1st mode (A) and 2nd mode (B) in ABAQUS.

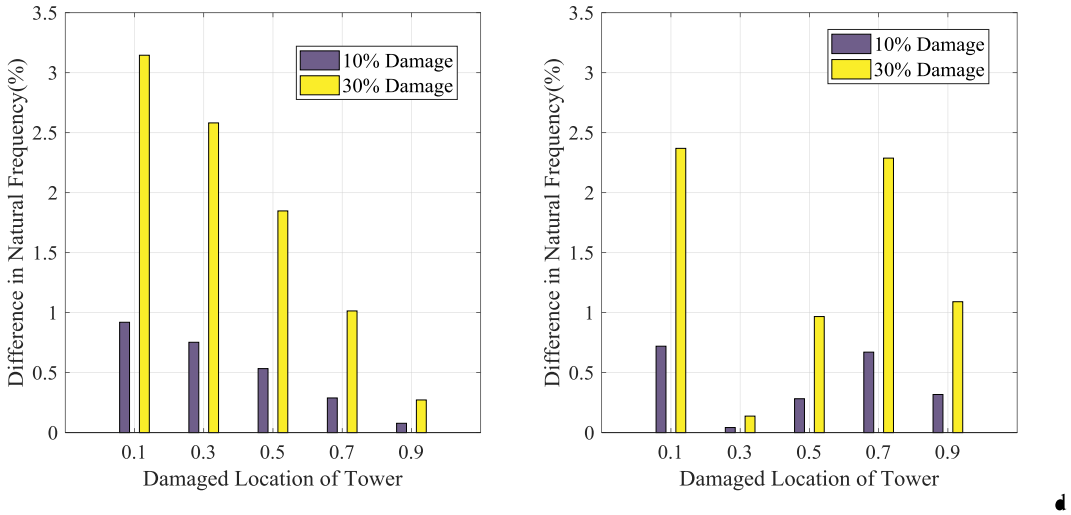

Fig. 16. Difference in natural frequencies of tower side-to-side 1st mode (A) and 2nd mode (B) in ABAQUS.

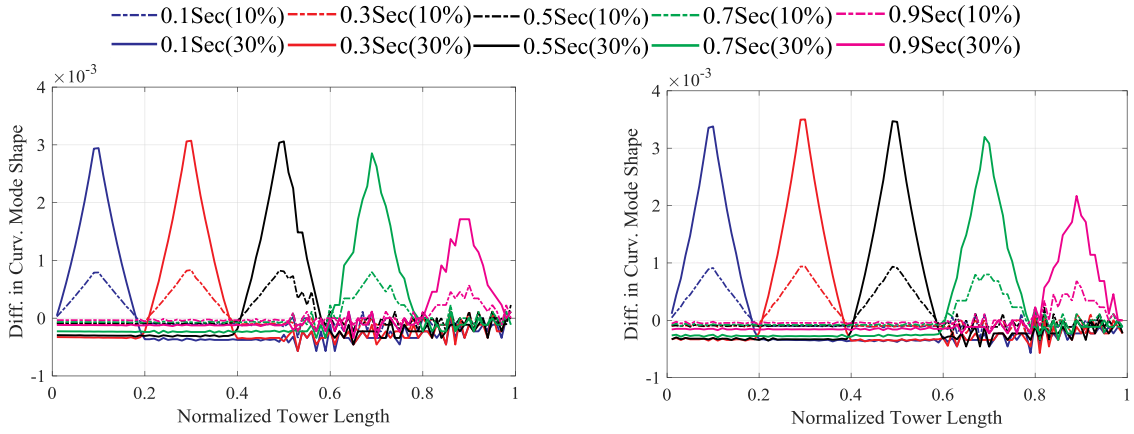

Fig. 17. Differences in CMS of 1st fore-aft tower mode (A) and side-to-side mode (B) of FOWT by FEM anlaysis

by FEM first. In the first fore-aft mode of the tower, the difference in natural frequency is the highest when the damage occurs at the 0.1 section. The difference decreases as the damaged location is higher, as shown in Fig. 15A. In the second fore-aft mode of the tower, the difference is high when the damage occurs at the 0.1 and 0.7 sections, whereas the difference is minimal when the damage occurs at the 0.3 section as shown in Fig. 15B. The trend is the same in the tower side-to-side mode, as shown in Fig. 16.

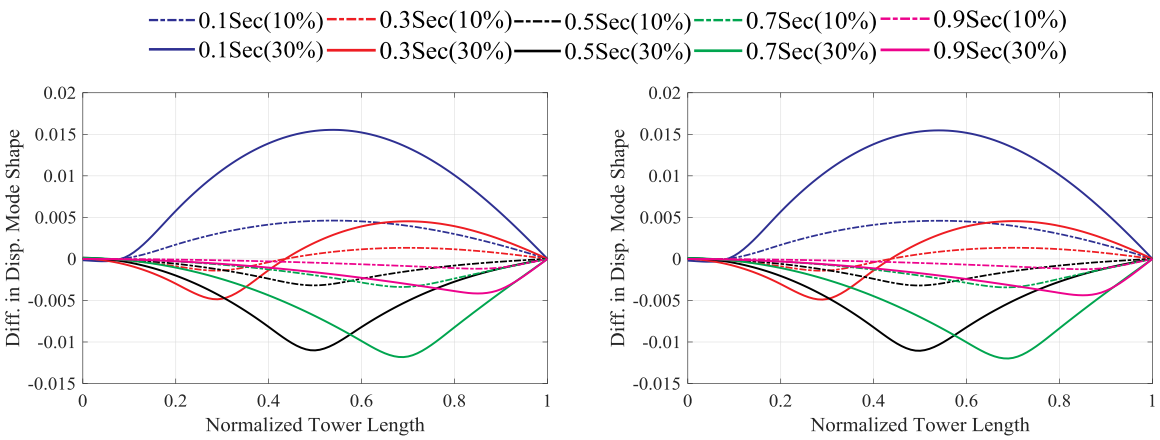

Fig. 18. Differences in DMS of 1st fore-aft tower mode (A) and side-to-side mode (B) of FOWT by FEM analysis.

Fig. 17 shows the differences in CMSs between intact and damaged conditions. In the figures, it is seen that a large difference in CMS develops in the damaged section, and thus the damaged location and intensity can be predicted through the difference. Fig. 18 also shows the same case when using DMS instead of CMS. It is seen that damage detection is very difficult by observing the difference in displacement-mode shape. This explains why the curvature-based method should be used in detecting damage. In the FEM analysis, 100 and 49 elements are used for the tower and blades, respectively.

4.3.3. Structural health monitoring of FOWT-tower using OMA

In this section, the natural frequencies and modal properties estimated by OMA are presented. The FEM-based mode shapes for intact and damaged conditions can be inputted for the fully-coupled FOWT dynamics simulation in the time domain to obtain the respective numerical-sensor signals. Then we can do OMA for both intact and damaged cases. They are compared, and their differences are presented in the following. As for natural frequencies and modal properties, a similar pattern shown in the FEM results (Figs. 15–18) is also found in the OMA results although there exist nontrivial differences between them as shown in Fig. 19 ~ Fig. 20. Fig. 21 shows the differences in CMSs of fore-aft tower mode and side-to-side tower mode, respectively. The damaged location can be predicted through the differences because significant peaks in the differences of CMSs mean damaged region. Besides, the damaged intensity can also be predicted through the magnitude of difference in the CMS, as demonstrated in the figures. In the OMA results in Fig. 21, the pattern of peaks as the indication of damaged location and degree is less clear than the FEM cases, especially when the damage is less than 10%. However, there is still no problem in detecting the damage location and degree by monitoring the difference in natural frequencies of side-to-side second tower mode and CMS of side-to-side first tower mode as shown in Figs. 20B and 21B. The above discussion shows that by continuously analyzing the differences of sensor signals by OMA, damage detection can be made.

Fig. 22 shows the differences in the exemplary numerical-accelerometer signals and its PSD between the intact case and 30% damaged case of the FOWT tower. The numerical sensor #5 is at normalized length 0.1 above the tower base. The damage causes changes in time series and shifts (blue circles: from 2.30 rad/sec to 2.24 rad/sec and from 18.59 rad/sec to 18.12 rad/sec) of natural frequencies in the PSD. The natural frequencies correspond to the first and second side-to-side tower modes.

4.3.4. Structural health monitoring of FOWT-blade using OMA

In this section, we consider the SHM of FOWT blades under the same environmental condition, and the upright blade among three blades is selected. To monitor the status of the upright blade using OMA, 19 numerical sensors are installed along the blade length, and the normalized locations of sensors are tabulated in Table 5. By applying the OMA technique to the numerical sensor signals, the 1st and 2nd flap modes and the 1st edge modes are captured. Among those

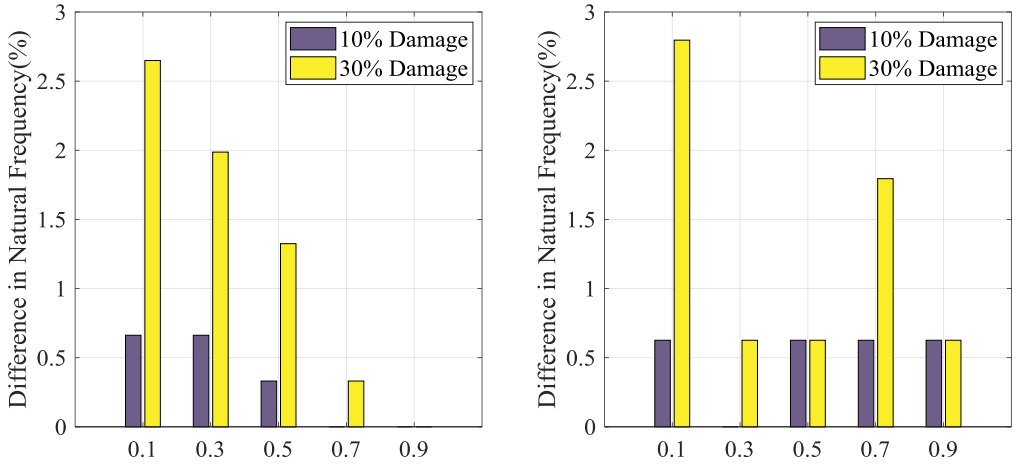

Fig. 19. Difference in natural frequencies of tower fore-aft 1st mode (A) and 2nd mode (B) of FOWT in OMA.

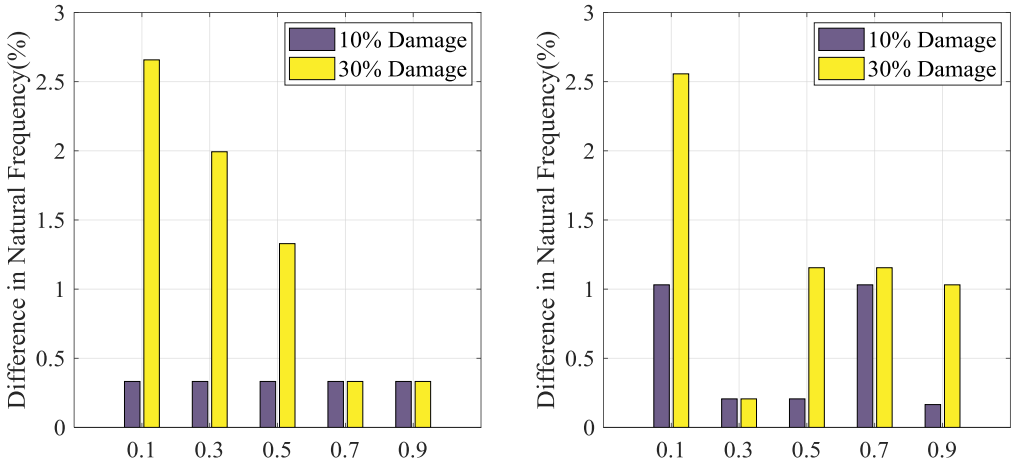

Fig. 20. Difference in natural frequencies of tower side-to-side 1st mode (A) and 2nd mode (B) of FOWT in OMA.

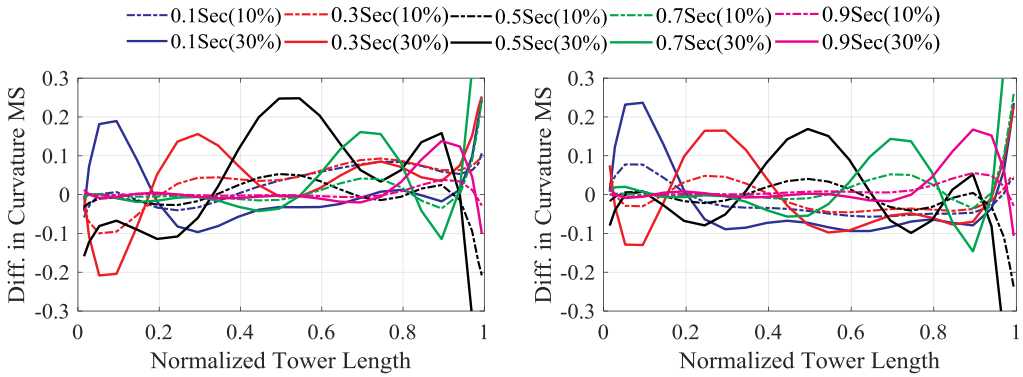

Fig. 21. Difference in CMS of 1st tower mode in FOWT: fore-aft (A) and side-to-side (B) by OMA.

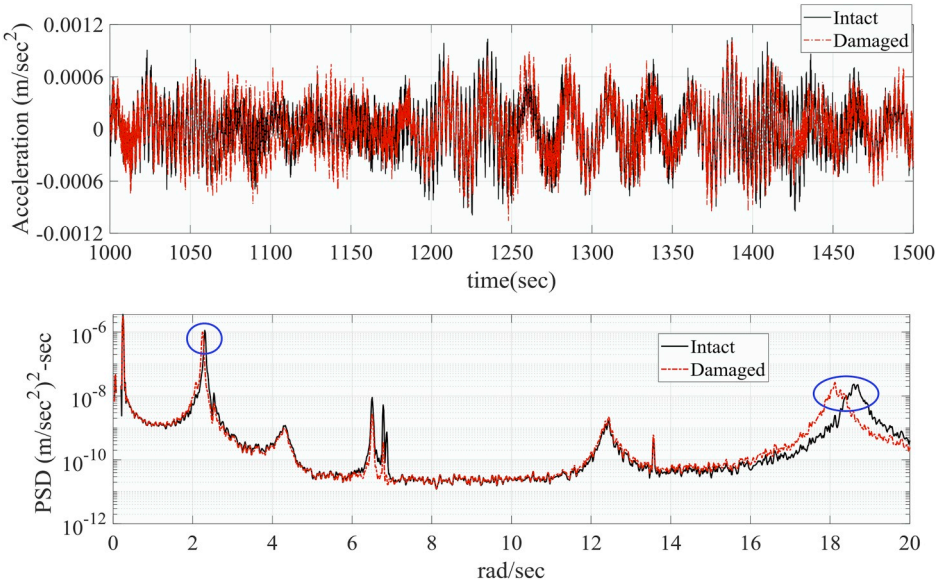

Fig. 22. Time series (A) and log-scaled PSD (B) of side-to-side acceleration signals from numerical sensor #5 on the tower, which is located at normalized length 0.1 above tower base, between the intact case and 30% damaged case of FOWT.

blade modes, the edge modes are the most appropriate to use for health monitoring due to a more noticeable appearance. Fig. 23A shows the entire mode spectrum obtained from the blade signals of edge-direction. In the 1st blade edge mode, three neighboring peaks (for edge-symmetry, edge-pitch, and edge-yaw modes) are generated, as shown in Fig. 23B.

Table 8 shows the comparison of natural frequencies of blade modes between ABAQUS (FEM) and FAST-CHARM3D (OMA), and their results

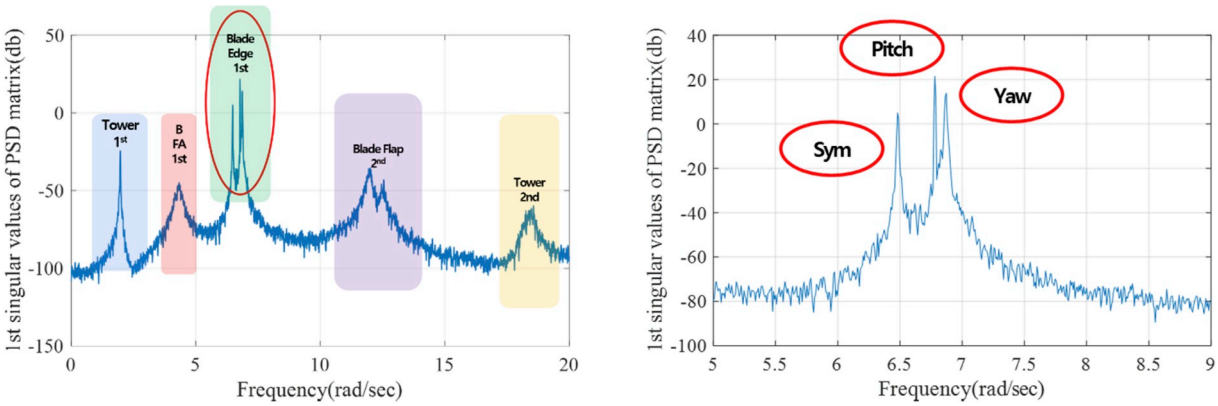

Fig. 23. Entire modes (A) and three-fold blade-1st-edge modes (B) obtained from edge-direction blade signals (B is the expansion of the circled region of A).

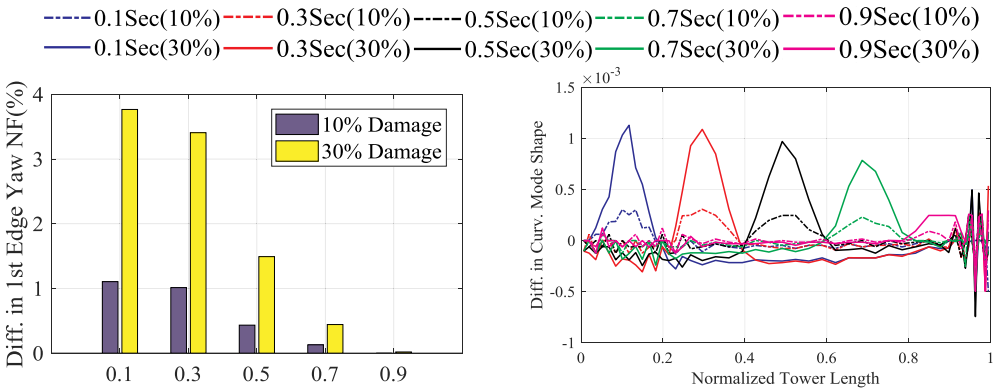

Fig. 24. Difference (between intact and damaged) in natural frequency (A) and CMS of upright blade's 1st edge-yaw mode of FOWT (B) by FEM.

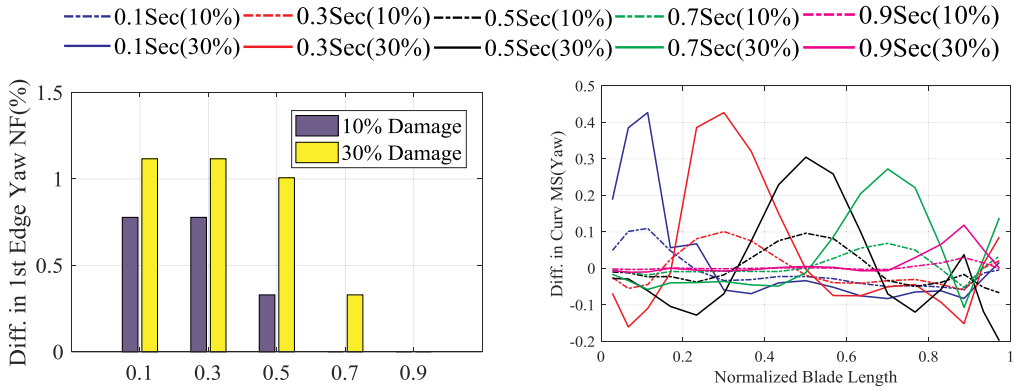

Fig. 25. Difference in natural frequency (A) and CMS of upright blade's 1st edge-yaw mode of FOWT (B) by OMS between intact and damaged cases.

agree well with each other. It means that the present OMA can catch the blade modes well even for the FOWT. Fig. 24 shows the differences in natural frequencies (A) and CMSs (B) obtained from the FEM analysis. Like the tower case, the damaged location can be found by the difference in CMS, and the pattern of difference in blade natural frequencies is very similar to that of the 1st mode of tower. Fig. 25 shows the corresponding results of Fig. 24 when the OMA is used instead of FEM. The general trend is very similar between the two. This means that blade damage can also be detected from the recorded sensor signals using the present OMA-CMS algorithm.

5. Conclusions

In this study, the feasibility to detect the damage on the blade and tower of FOWT using OMA and difference in modal properties was examined. The modal properties were obtained by applying OMA from the signals of numerical sensors on blade and tower. The numerical sensor signals were obtained using a turbine-floater-mooring fully-coupled dynamics simulation program in the time domain, which has been extensively validated through comparisons with experiments by authors in the previous papers. Also, the OMA results were also self-checked against independent FEM results. The locally damaged conditions were modeled by reducing the local structural stiffness. Then, it was observed that the local damage could be effectively detected using OMA and CMS, which improve the performance of the damage detection compared to the method using DMS. It was also confirmed that the general trend of differences between intact and damaged cases by FEM agreed well to those obtained from OMA with numerical-sensor signals

for a FOWT.

The considerable differences in CMSs between intact and damaged conditions at the damaged location were displayed. The differences increased with the degree of damage. The similarity in the pattern of FEM/OMA results between on-land and floating wind turbines was explained. It was also seen that the deduced modal properties of the FOWT by OMA were negligibly affected by the mooring non-linearity or/and additional wave environments. When it comes to the coupling effect between the tower and blades, the rotor coupled effect on the tower affects much the modal properties of the tower while the tower coupled effect on the blade is negligible in the first and second blade modes. The present numerical-simulation and damage-detecting method may be used to build up a huge database for various damage scenarios and the corresponding patterns of tower-blade dynamic behaviors so that it can be applied to machine-generated and machine-learning SHM technology in the future.

Acknowledgment

This material is based upon work supported by the National Science Foundation (Grant # 1700406), and this work was also partly supported by the National Research Foundation of Korea (NRF) grant funded by the Korea government (MSIT) (Grant # 2017R1A5A1014883).

References

Bae, Y.H., Kim, M.H., 2013. Influence of failed blade-pitch-control system to FOWT by aero-elastic-control-floater-mooring coupled dynamic analysis. Ocean Syst. Eng. 3 (4), 295–307.
Bae, Y.H., Kim, M.H., 2014. Coupled dynamic analysis of multiple wind turbines on a large single floater. Ocean. Eng. 92, 175–187.
Bae, Y.H., Kim, M.H., 2014. Influence of control strategy on FOWT global performance by aero-elastic-control-floater-mooring coupled dynamic analysis. J. Ocean. Wind Energy 1 (1), 50–58.
Bae, Y.H., Kim, M.H., Kim, H.C., 2017. Performance changes of a floating offshore wind turbine with broken mooring line. Renew. Energy 101, 364–375.
Bir, G., Jonkman, J.M., 2007. Aeroelastic instabilities of large offshore and onshore wind turbines. In: Journal of Physics: Conference Series. IOP Publishing.
Brincker, R., Zhang, L., Andersen, P., 2001. Modal identification of output-only systems using frequency domain decomposition. Smart Mater. Struct. 10 (3), 441.
Brownjohn, J., Pavic, A., Carden, E., Middleton, C., 2007. Modal Testing of Tamar Suspension Bridge.
Brownjohn, J., Magalhaes, F., Caetano, E., Cunha, A., 2010. Ambient vibration re-testing and operational modal analysis of the Humber Bridge. Eng. Struct. 32 (8), 2003–2018.
Chauhan, S., Tcherniak, D., Basurko, J., Salgado, O., Urresti, I., Carcangiu, C.E., Rossetti, M., 2011. Operational modal analysis of operating wind turbines: application to measured data. In: Rotating Machinery, Structural Health Monitoring, Shock and Vibration, 5, pp. 65–81.
Ciang, C.C., Lee, J.-R., Bang, H.-J., 2008. Structural health monitoring for a wind turbine system: a review of damage detection methods. Meas. Sci. Technol. 19 (12), 122001.
Conte, J.P., He, X., Moaveni, B., Masri, S.F., Caffrey, J.P., Wahbeh, M., Tasbihgoo, F., Whang, D.H., Elgamal, A., 2008. Dynamic testing of Alfred Zampa memorial bridge. J. Struct. Eng. 134 (6), 1006–1015.
Devriendt, C., Elkafafy, M., De Sitter, G., Guillaume, P., 2012. Continuous dynamic monitoring of an offshore wind turbine on a monopile foundation. In: International Conference on Noise and Vibration Engineering. ISMA, Leuven.
Devriendt, C., Jordaens, P., Sitter, G., Guillaume, P., 2013. Damping estimation of an offshore wind turbine on a monopile foundation. IET Renew. Power Gener. 7 (4), 401–412.
Devriendt, C., Magalhães, F., Weijtjens, W., De Sitter, G., Cunha, Á., Guillaume, P., 2014. Structural health monitoring of offshore wind turbines using automated operational modal analysis. Struct. Health Monit. 13 (6), 644–659.
Griffith, D.T., Yoder, N., Resor, B., White, J., Paquette, J., 2012. Structural Health and Prognostics Management for Offshore Wind Turbines: An Initial Roadmap. SAND2012-10109. Sandia National Laboratories.
Hameed, Z., Hong, Y., Cho, Y., Ahn, S., Song, C., 2009. Condition monitoring and fault detection of wind turbines and related algorithms: a review. Renew. Sustain. Energy Rev. 13 (1), 1–39.
Hu, W.-H., Thöns, S., Rohrmann, R.G., Said, S., Rücker, W., 2015. Vibration-based structural health monitoring of a wind turbine system Part II: environmental/operational effects on dynamic properties. Eng. Struct. 89, 273–290.
Jonkman, B.J., 2009. TurbSim User's Guide: Version 1.50. National Renewable Energy Lab.(NREL), Golden, CO (United States).
Jonkman, J.M., Butterfield, S., Musial, W., Scott, G., 2009. Definition of a 5-MW Reference Wind Turbine for Offshore System Development. National Renewable Energy Laboratory (NREL), Golden, CO.
Kim, H.C., Kim, M.H., 2015. Global performances of a semi-submersible 5MW wind-turbine including second-order wave-diffraction effects. Ocean Syst. Eng. 5 (3), 139–160.
Kim, S., Adams, D.E., Sohn, H., Rodriguez-Rivera, G., Myrent, N., Bond, R., Vitek, J., Carr, S., Grama, A., Meyer, J.J., 2014. Crack detection technique for operating wind turbine blades using Vibro-Acoustic Modulation. Struct. Health Monit. 13 (6), 660–670.
Kim, Y., Ahn, I.-G., Park, S.-G., 2015. Extraction of the mode shapes of a segmented ship model with a hydroelastic response. Int. J. Nav. Archit. Ocean. Eng. 7 (6), 979–994.
Kim, H.C., Kim, K.H., Kim, M.H., Hong, K., 2017. Global performance of a KRISO semisubmersible multiunit floating offshore wind turbine: numerical simulation vs. Model test. Int. J. Offshore Polar Eng. 27 (01), 70–81.
Levitt, A.C., Kempton, W., Smith, A.P., Musial, W., Firestone, J., 2011. Pricing offshore wind power. Energy Policy 39 (10), 6408–6421.
Liu, F., Li, H., Hu, S.-L.J., 2015. Stochastic modal analysis for a real offshore platform. In: Proceedings of the 6th International Operational Modal Analysis Conference, Gijón, Spain.
Di Lorenzo, E., Manzato, S., Peeters, B., Van der Auweraer, H., 2013. Virtual structural monitoring of wind turbines using Operational Modal Analysis techniques. In: Key Engineering Materials. Trans Tech Publ.
Di Lorenzo, E., Petrone, G., Manzato, S., Peeters, B., Desmet, W., Marulo, F., 2016. Damage detection in wind turbine blades by using operational modal analysis. Struct. Health Monit. 15 (3), 289–301.
Magalhães, FMRLd, 2012. Operational Modal Analysis for Testing and Monitoring of Bridges and Special Structures.
Manzato, S., White, J.R., LeBlanc, B., Peeters, B., Janssens, K., 2014. Advanced identification techniques for operational wind turbine data. In: Topics in Modal Analysis, vol. 7. Springer, pp. 195–209.
Mieloszyk, M., Opoka, S., Ostachowicz, W., 2015. Frequency Domain Decomposition performed on the strain data obtained from the aluminium model of an offshore support structure. In: Journal of Physics: Conference Series. IOP Publishing.
Moné, C., Hand, M., Bolinger, M., Rand, J., Heimiller, D., Ho, J., 2015. *Cost* of Wind Energy Review, vol.2017.
Osgood, R., Bir, G., Mutha, H., Peeters, B., Luczak, M., Sablon, G., 2011. Full-scale modal wind turbine tests: comparing shaker excitation with wind excitation. In: Structural Dynamics and Renewable Energy, vol. 1. Springer, pp. 113–124.
Pandey, A., Biswas, M., Samman, M., 1991. Damage detection from changes in curvature mode shapes. J. Sound Vib. 145 (2), 321–332.
Ruzzo, C., Failla, G., Collu, M., Nava, V., Fiamma, V., Arena, F., 2016. Operational modal analysis of a spar-type floating platform using frequency domain decomposition method. Energies 9 (11), 870.
Sainz, E., Llombart, A., Guerrero, J., 2009. Robust filtering for the characterization of wind turbines: improving its operation and maintenance. Energy Convers. Manag. 50 (9), 2136–2147.
Schulz, M.J., Ghoshal, A., Sundaresan, M.J., Pai, P.F., Chung, J.H., 2003. Theory of damage detection using constrained vibration deflection shapes. Struct. Health Monit. 2 (1), 75–99.
Shokrieh, M.M., Rafiee, R., 2006. Simulation of fatigue failure in a full composite wind turbine blade. Compos. Struct. 74 (3), 332–342.
Siebel, T., Friedman, A., Koch, M., Mayer, D., 2012. Assessment of mode shape-based damage detection methods under real operational conditions. In: 6th European Workshop on Structural Health Monitoring. Dresden, Germany.
De Sitter, G., Weitjens, W., El-Kafafy, M., Devriendt, C., 2013. Monitoring changes in the soil and foundation characteristics of an offshore wind turbine using automated operational modal analysis. In: Key Engineering Materials. Trans Tech Publ.
Sørensen, B.F., Jørgensen, E., Debel, C.P., Jensen, H.M., Jacobsen, T.K., Halling, K., 2004. Improved Design of Large Wind Turbine Blade of Fibre Composites Based on Studies of Scale Effects (Phase 1). Summary Report.
Tcherniak, D., Larsen, G.C., 2013. Application of OMA to an operating wind turbine: now including vibration data from the blades. In: 5th International Operational Modal Analysis Conference.
Tcherniak, D., Chauhan, S., Hansen, M.H., 2011. Applicability limits of operational modal analysis to operational wind turbines. In: Structural Dynamics and Renewable Energy, vol.1. Springer, pp. 317–327.
Van der Valk, P.L., Ogno, M.G., 2014. Identifying structural parameters of an idling offshore wind turbine using operational modal analysis. In: Dynamics of Civil Structures, vol. 4. Springer, pp. 271–281.
Wang, Y., Liang, M., Xiang, J., 2014. Damage detection method for wind turbine blades based on dynamics analysis and mode shape difference curvature information. Mech. Syst. Signal Process. 48 (1), 351–367.
Weijtjens, W., Verbelen, T., Capello, E., Devriendt, C., 2017. Vibration based structural health monitoring of the substructures of five offshore wind turbines. Procedia Eng. 199, 2294–2299.
White, J.R., 2010. Operational Monitoring of Horizontal axis Wind Turbines with Inertial Measurements. Purdue University.